AD-A093 026 ROME AIR DEVELOPMENT CENTER GRIFFISS AFB NY F/G 20/14
COMSTAR MILLIMETER-WAVE PROPAGATION MEASUREMENTS,(U)
APR 80 L E TELFORD
UNCLASSIFIED RADC-TR-80-133 NL

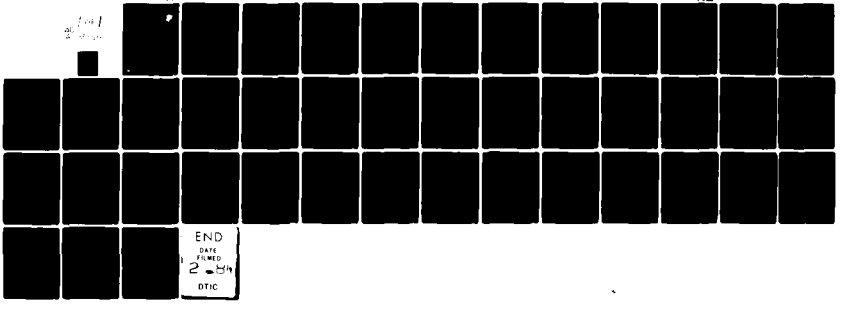

END
DATE FILMED
2-81
DTIC

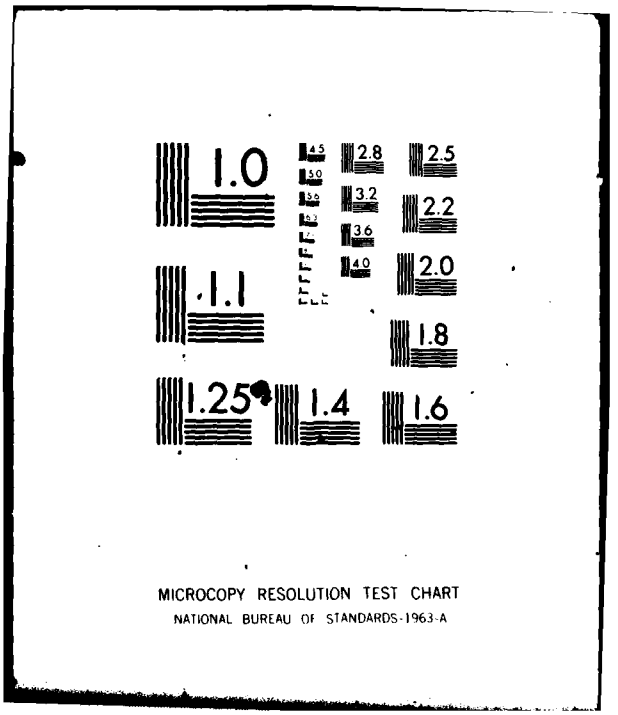
1.0
1.1
1.25
1.4
1.6
1.8
2.0
2.2
2.5
2.8
3.2
3.6
4.0
4.5
5.0
5.6
MICROCOPY RESOLUTION TEST CHART
NATIONAL BUREAU OF STANDARDS-1963-A

RADC-TR-80-133
In-House Report
April 1980

LEVEL II

COMSTAR MILLIMETER-WAVE PROPAGATION MEASUREMENTS

Larry E. Telford

ROME AIR DEVELOPMENT CENTER
Air Force Systems Command
Griffiss Air Force Base, New York 13441

This report has been reviewed by the RADC Public Affairs Office (PA) and is releasable to the National Technical Information Service (NTIS). At NTIS it will be releasable to the general public, including foreign nations.

RADC-TR-80-133 has been reviewed and is approved for publication.

APPROVED: Edward A. Lewis
EDWARD A. LEWIS, Chief
Propagation Branch
Electromagnetic Sciences Division

APPROVED: Allan C. Schell
ALLAN C. SCHELL, Chief
Electromagnetic Sciences Division

FOR THE COMMANDER: John P. Huss
JOHN P. HUSS
Acting Chief, Plans Office

If your address has changed or if you wish to be removed from the RADC mailing list, or if the addressee is no longer employed by your organization, please notify RADC (EEP), Hanscom AFB MA 01731. This will assist us in maintaining a current mailing list.

Do not return this copy. Retain or destroy.

MISSION
of
Rome Air Development Center

RADC plans and executes research, development, test and selected acquisition programs in support of Command, Control Communications and Intelligence (C^3I) activities. Technical and engineering support within areas of technical competence is provided to ESD Program Offices (POs) and other ESD elements. The principal technical mission areas are communications, electromagnetic guidance and control, surveillance of ground and aerospace objects, intelligence data collection and handling, information system technology, ionospheric propagation, solid state sciences, microwave physics and electronic reliability, maintainability and compatibility.

Printed by
United States Air Force
Hanscom AFB, Mass. 01731

Unclassified

SECURITY CLASSIFICATION OF THIS PAGE (When Data Entered)

REPORT DOCUMENTATION PAGE	READ INSTRUCTIONS BEFORE COMPLETING FORM
1. REPORT NUMBER: RADC-TR-80-133 (14)	2. GOVT ACCESSION NO.: AD-A093026
3. RECIPIENT'S CATALOG NUMBER	
4. TITLE (and Subtitle): COMSTAR MILLIMETER-WAVE PROPAGATION MEASUREMENTS (6)	5. TYPE OF REPORT & PERIOD COVERED: In-house
	6. PERFORMING ORG. REPORT NUMBER
7. AUTHOR(s): Larry E. Telford (10)	8. CONTRACT OR GRANT NUMBER(s)
9. PERFORMING ORGANIZATION NAME AND ADDRESS: Deputy for Electronic Technology (RADC/EEP) Hanscom AFB Massachusetts 01731	10. PROGRAM ELEMENT, PROJECT, TASK AREA & WORK UNIT NUMBERS: 62702F (16) 46001601 (11) (16)
11. CONTROLLING OFFICE NAME AND ADDRESS: Deputy for Electronic Technology (RADC/EEP) Hanscom AFB Massachusetts 01731	12. REPORT DATE: Apr 1980 (11) 13. NUMBER OF PAGES: 43 (12)
14. MONITORING AGENCY NAME & ADDRESS (if different from Controlling Office)	15. SECURITY CLASS. (of this report): Unclassified 15a. DECLASSIFICATION DOWNGRADING SCHEDULE

16. DISTRIBUTION STATEMENT (of this Report)

Approved for public release; distribution unlimited.

17. DISTRIBUTION STATEMENT (of the abstract entered in Block 20, if different from Report)

18. SUPPLEMENTARY NOTES

19. KEY WORDS (Continue on reverse side if necessary and identify by block number)

Satellite communication systems
Millimeter-wave propagation
Rain attenuation

20. ABSTRACT (Continue on reverse side if necessary and identify by block number)

The use of millimeter frequencies for earth-to-space communication links will soon be a reality. It has been long known that precipitation will be a problem because of the relatively large attenuation caused by rainfall along the propagation path. Some of the latest experiments to provide needed propagation data have involved the COMSTAR Millimeter-Wave Beacons which were part of three synchronous orbit satellites launched by COMSAT Laboratories. The Propagation Branch of the Electromagnetic Sciences Division

DD FORM 1 JAN 73 1473 EDITION OF 1 NOV 65 IS OBSOLETE

Unclassified

SECURITY CLASSIFICATION OF THIS PAGE (When Data Entered)

30150

TCD

20. Abstract (Continued)

utilized these beacons to obtain attenuation ratio data at 19 and 28 GHz and phase dispersion data at 28 GHz. This report is a station report covering the 1-year measurement program and various theoretical analyses. The attenuation ratio data was in fair agreement with the theory; however, considerable variation was found at low attenuations. Phase dispersion measurements were in reasonable agreement with theory considering the small magnitude of the phase dispersion across a 1 GHz bandwidth at 28 GHz. From a practical point of view, for a given propagation path, the path attenuation will be very large before phase dispersion becomes a problem for most systems.

Preface

The author would like to thank his co-workers, J. Frazier and W. Taffe for the design and construction of the antenna interface and J. Doherty for his programming assistance in the reading of the data magnetic tapes.

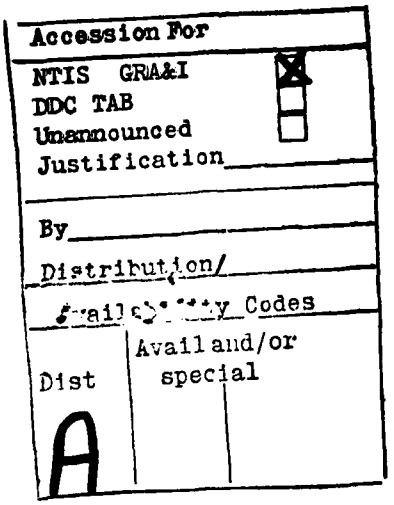

Contents

Illustrations

Illustrations

Tables

COMSTAR Millimeter-Wave Propagation Measurements

1. INTRODUCTION

The use of the millimeter-wave portion of the electromagnetic spectrum for earth-to-space communications has been predicted for many years. The rapid expansion of the utilization of the lower frequency bands, mainly 4 GHz and 6 GHz, has led to the desire to move upwards in frequency. The availability of 2000 MHz of bandwidth in the 20-GHz and 30-GHz bands vs the 500 MHz available at 4 and 6 GHz (as well as freedom from interference problems with terrestrial communication links) has generated great interest in the millimeter wave bands in recent years. Other potential advantages to the use of millimeter waves for earth-to-space communications include the possibility of using smaller antennas, and essentially no interaction with the ionosphere. The wider bandwidths also mean greater data rates can be transmitted per satellite channel. The great disadvantage to using millimeter waves for satellite communications as well as for terrestrial links is the large attenuation due to rain. The normal error budget for rain at 4 and 6 GHz is less than 2 dB, while moderate rain can easily cause attenuations exceeding 30 dB at 20 and 30 GHz. The ultimate effect of such attenuations is the reduced availability for single-station operation or the requirement to use more than one ground station in a space diversity mode. The characterization of the effects of rain on

(Received for publication 22 April 1980)

millimeter waves has been examined both theoretically and experimentally since the early 1940's.

The lack of a suitable millimeter-wave beacon on a spacecraft limited early rain attenuation measurements either to radiometric observations using the sun as a source or to the determination of attenuation from the radiometric emission of the rain itself. The details and limitations of these methods have been covered in the literature.[1] Basically, the radiometric methods suffered from a lack of dynamic range in the case of the passive method and a source which is continually moving in azimuth and elevation when using suntrackers. Two NASA research satellites, ATS-5 and ATS-6, offered the first opportunity to utilize millimeter-wave beacons on spacecraft. Both satellites were in synchronous orbit; therefore the position requirement of essentially constant elevation and azimuth was met. However, both experiments suffered from interruptions in the transmissions of the beacons. ATS-5 had orbit insertion problems and was spinning, which resulted in the received signal appearing as a pulsed signal with a corresponding loss of average signal level. This loss in dynamic range plus the limited beacon on time resulted in less than satisfactory outage statistics, but significant data were collected at the 15 GHz downlink frequency.[2,3] In addition, NASA collected some simultaneous 15- and 32-GHz attenuation data at the Rosman, North Carolina site. ATS-6 contained beacons at 20 and 30 GHz but also suffered from a constrained operating schedule. The spacecraft lacked sufficient power to allow all experiments to operate simultaneously, and at times spacecraft-pointing requirements also prevented the beacons from transmitting. The net result was interesting data collected both in the United States and Europe, but again a lack of the statistical data the communications people required.[4]

Bell Telephone Laboratories and COMSAT Laboratories combined resources to place three beacons on a series of planned domestic communication satellites to be launched in the late 1970's. These beacons, operating at 19.04 GHz and 28.56 GHz were designed to satisfy the communication system planners' requirements, leading to future implementation of 20/30 GHz satellite communication links. Sufficient power, about +55 dbm effective radiated power, and an operating schedule allowing at least 2 years continuous operation was the result. Dual linear

---

1. Hogg, D.C. and Chu, T. (1975) The role of rain in satellite communications, Proceedings of IEEE 63:1308-1331.
2. Ippolito, L.J. (1970) Millimeter-Wave Propagation Experiments Utilizing the ATS-5 Satellite, NASA Publication X-751-70-428, Goddard Space Flight Center.
3. Ippolito, L.J. (1972) Earth-Satellite Propagation Above 10 GHz, NASA Publication X-751-72-208, Goddard Space Flight Center, May.
4. Ippolito, L.J. (1976) 20- and 30-GHz Millimeter Wave Experiments With the ATS-6 Satellite, NASA Technical Note #D-8197, April, pp. 57-91.

polarizations were transmitted at 19 GHz and coherent sidebands on the 28 GHz carrier were available for phase-dispersion measurements. A total of three, two-frequency beacons were successfully launched and operated. The first two, designated D-1 and D-2, were launched in May and July of 1976. Both beacons operated until September 1978 when the power requirements of the parent spacecraft forced the shutdown of both beacons. Fortunately D-3, which was launched in July, 1978 was available to replace the earlier sources. Assuming the same 2-year life span for the D-3 beacon, over 4 years of continuous beacon operation at 19 GHz and 28 GHz will have been made available for propagation measurements.

The Propagation Branch of the Electromagnetic Sciences Division of RADC, having been involved in millimeter-wave propagation measurements since the early 1960's, participated in the COMSTAR Beacon program by establishing a ground receiver station at the Prospect Hill Millimeter Wave Facility located in Waltham, Massachusetts. The original intent was to measure 19- and 28-GHz carrier levels and the relative phase between the two 28-GHz sidebands and carrier for a sufficiently long period to collect meaningful statistics for the New England area. A two-frequency receiver was procured under contract and installed in an existing 18-foot parabolic antenna. Initial operation was in December, 1977 and continued until February, 1979 when due to an abnormal ice storm, the antenna mount failed, resulting in the destruction of the antenna. In addition, the data collected over the previous 13 months suffered from equipment problems and an abnormally low rainfall. As will be described in later sections, due to these difficulties, insufficient data were collected to establish meaningful percentage time statistics on the attenuation levels for the two frequencies. The ratios of the two attenuations during the various rain events and the phase variations of the 28-GHz sidebands do not require continuous data and the lack of normal rainfall did not affect these parameters adversely. This report will concentrate on the attenuation ratios and the phase variations of the 28-GHz sidebands measured during 1978. Attenuation ratios are useful for extending attenuation measurement results made at one millimeter frequency to other millimeter frequencies without the expense of acquiring additional equipment. Phase dispersion, if large, could affect future high data rate digitial satellite communication links.

The report is organized into five sections including the Introduction. Section 2 will consider the theoretical aspects of the ratio of attenuations and the phase dispersion. The experimental configuration is discussed in Section 3. Section 4 describes the data analysis and results, and Section 5 contains conclusions of the report.

2. THEORETICAL CONSIDERATIONS

The ability to calculate the attenuation due to rain has existed for many years.[5, 6, 7] The calculations are complex, requiring large computers and are not easily used by system designers. The poor comparison of available experimental attenuation data to the theoretical results in Medhurst's paper[5] led him to be skeptical of the applicability of the theory. However, later investigations and experiments have shown the theoretical calculations to be correct. It is generally accepted that the early discrepancies were due to inadequate rain-rate sampling and the lack of spatial rain uniformity along the paths used. Crane[8] has shown that precise characterization of the raindrop distribution, shape, and size (along with the use of a short path to assure a uniform rain rate) will produce results which agree with the theoretical calculations. To simplify the theoretical calculations, it has been noted by many authors that an expression of the form

$$A = aR^b \tag{1}$$

where

A = attenuation in db/km

R = rain rate in mm/hr

a, b = empirical constants

can be used to calculate the attenuation given the rain rate. The constants a and b are functions of frequency and the dropsize distribution chosen to represent the local rainfall. Olsen, et al[9] have provided a theoretical justification for use of expressions of the form of Eq. (1) for rain attenuation and have presented tables and graphs of a and b for several dropsize distributions. In addition, the limitations of using Eq. (1) in comparison to using the full Mie scattering calculations are discussed. Essentially, the difference between results derived from Eq. (1)

---

5. Medhurst, R.G. (1965) Rainfall attenuation of centimeter waves: comparison of theory and measurement, IEEE Transactions on Antennas and Propagation, AP-13, pp. 550-564.
6. Oguchi, T. (1964) Attenuation of electromagnetic wave due to rain with distorted raindrops (part II), Journal Radio Research Laboratories 11:19-44.
7. Setzer, D.E. (1970) Computed transmission through rain at microwave and visible frequencies, Bell System Technical Journal 49:1873-1892.
8. Crane, R.K. (1974) The rain range experiment—propagation through a simulated rain environment, IEEE Transactions on Antennas and Propagation, AP-22, pp. 321-328.
9. Olsen, R.L., Rogers, D.V., and Hodge, D.B. (1978) The aRb relation in the calculation of rain attenuation, IEEE Transactions on Antennas and Propagation, AP-26, pp. 318-329.

and results derived from Mie scattering theory are sufficiently small so that for most purposes, Eq. (1) is more than adequate.

Attenuation measurements made on an earth-to-space path do not satisfy the short path and uniform rain-rate criteria discussed earlier. Raindrop shape, size, and distribution along the path can never be adequately measured and there is no easy method for choosing a correct distribution for use in calculating attenuations along such a path. The question generally reduces to a choice of the dropsize distribution which best fits the available data.

Attenuation ratios from calculated attenuations using several dropsize distributions were examined. First, ratios were calculated using Medhurst's artificial rain composed of drops of equal diameter. In calculations using distributions consisting of equal size, spherical drops are perhaps the least realistic, but they do provide some measure of the range of attenuation ratios to be expected. Table 1 is a listing of the 19.04-GHz and 28.56-GHz attenuations in db/km as interpolated from Table 4 of Medhurst's paper. Dropsizes from 0.05 cm to 0.70 cm in diameter are included which more than encompass the types of rain normally experienced. The 28.5-GHz to 19.04-GHz attenuation ratios vary from a high of 2.94 for a 0.1-cm drop diameter to a low of 0.98 for very large drops. Note that the drops are assumed to be spherical and the rain temperature is assumed to be 20°C. The data in Table 1 indicate a decreasing attenuation for drops with diameters greater than 0.25 cm; however, it should be kept in mind that a constant rain rate of 1 mm/hr is assumed for all cases. A collection of small, uniformly distributed drops producing a rain rate of 1 mm/hr will have a greater attenuation than a collection of fewer, large diameter drops producing the same rain rate. In this case, the attenuation per drop will increase with dropsize for drops within the 0.05- to 0.7-cm diameter range.[10]

After seeing the fairly wide spread of ratios using the constant-diameter rain of Medhurst, ratios using more common dropsize distributions were examined. The source for the attenuation values was Tables I, II and III of Olsen, et al,[9] since they provided calculations for four different dropsize distributions at three temperatures and at 41 frequencies between 1 and 1000 GHz. The approach Olsen followed was to calculate the attenuation values using the Mie scattering theory for water spheres for each frequency, dropsize distribution, and temperature. Then, tables of the parameters a and b in Eq. (1) were obtained by means of a logarithmic regression for each combination of dropsize distribution, frequency, and temperature. The use of spherical waterdrops instead of actual, oblate raindrops resulted in less than an 8 percent error in attenuations for frequencies above

---

10. Altshuler, E.E. and Telford, L.E. (1980) Frequency Dependence of Slant Path Rain Attenuations at 15 and 35 GHz, paper submitted to Radio Science.

Table 1. Attenuations and Ratios of Attenuations at 19.04 GHz and 28.56 GHz for Constant-Diameter Raindrop Distributions

Drop Diameter (cm)	19 GHz Att (db/km)	28 GHz Att (db/km)	Ratio
0.05	0.038	0.089	2.35
0.10	0.042	0.125	2.94
0.15	0.070	0.179	2.54
0.20	0.108	0.208	1.93
0.25	0.102	0.206	2.02
0.30	0.100	0.201	2.01
0.35	0.102	0.169	1.66
0.40	0.104	0.144	1.38
0.45	0.115	0.120	1.04
0.50	0.105	0.110	1.05
0.55	0.093	0.099	1.06
0.60	0.086	0.091	1.06
0.65	0.085	0.083	0.98
0.70	0.077	0.077	1.00

Rain rate is 1 mm/hr for all cases.
Drops are of equal diameter.
Temperature is 20°C.

10 GHz according to Olsen. However, the known difference in vertically and horizontally polarized attenuations is not apparent when using spherically shaped drops. This lack of polarization differential is not a factor in this report. The adjustment to Olsen's tabulated values referred to in the footnote on page 322 of his paper was not incorporated in this analysis. Basically, the tabulated values are the result of several approximations and the distributions are only rough approximations to actual rain, therefore the errors caused by ignoring the adjustments are small in comparison.

Two of the dropsize distributions, Laws and Parsons (LP) and Marshall-Palmer (MP), are both considered to be reasonable choices for rain models in continental temperate climates. Both distributions were developed over 30 years ago and both have been widely tested and used in many previous calculations. Calculated attenuation ratios using these distributions will be seen to be very similar. Two other distributions, the Joss Thunderstorm (JT) and Joss Drizzle (JD)[11]

11. Joss, J., Thams, J.C., and Waldvogel, A. (1968) The variation of raindrop size distributions at Locarno, Proceedings of the International Conference on Cloud Physics, Toronto, Canada, pp. 369-373.

were included in the calculations performed by Olsen. The JT distribution was fitted to the "average" dropsize spectrum in convective rain and has been used for some specific attenuation calculations.[12, 13] The JD distribution was fitted to very light, widespread rain or drizzle and emphasized small drops.

Using data from Olsen's paper, values for the parameters a and b of Eq. (1) were obtained by fitting a power curve to the tabulated data to interpolate to the 19.04-GHz and 28.56-GHz frequencies. Twelve sets of parameters, including three temperatures for each of the four dropsize distributions, were obtained in this manner. Each set of parameters was used to calculate attenuation in db/km at each frequency for several rain rates by using the parameters in Eq. (1). Table 2 lists the attenuations and the attenuation ratios for each of the four dropsize distributions at a temperature of $0^{\circ}C$. Rain rates from 0.25 mm/hr to 100 mm/hr are included and the LP data are a combination of the LPL and LPH data as compiled by Olsen with the transition occurring at 30 mm/hr.

Table 2. Attenuations and Ratios of Attenuation at 19.04 GHz and 28.56 GHz as a Function of Dropsize Distribution and Rain Rate

Distribution Rain Rate (mm/hr)	Attenuation (19 GHz/28 GHz) (db/km)				Attenuation Ratio			
	LP	MP	JT	JD	LP	MP	JT	JD
0.25	0.012/0.033	0.014/0.039	0.023/0.033	0.012/0.027	2.82	2.79	3.22	2.34
0.50	0.025/0.069	0.030/0.080	0.044/0.132	0.023/0.056	2.71	2.69	2.99	2.39
1.00	0.055/0.144	0.064/0.166	0.085/0.235	0.047/0.115	2.60	2.60	2.77	2.44
2.00	0.120/0.301	0.137/0.344	0.164/0.421	0.096/0.237	2.50	2.52	2.57	2.48
5.00	0.336/0.798	0.374/0.899	0.391/0.910	0.242/0.617	2.37	2.41	2.33	2.55
10.0	0.731/1.668	0.800/1.859	0.754/1.629	0.490/1.270	2.28	2.32	2.16	2.60
20.0	1.589/3.486	1.712/3.846	1.455/2.915	0.989/2.616	2.19	2.25	2.00	2.60
50.0	4.449/9.099	4.682/10.06	3.469/6.294	2.501/6.794	2.05	2.15	1.82	2.72
100.	9.459/17.99	10.02/20.81	6.694/11.27	5.050/13.99	1.90	2.08	1.68	2.77

Temperature is 0 C

12. Llewellyn-Jones, D.T. (1973) Attenuation by rainfall in the submillimetre wave region, Modern Topics in Microwave Propagation and Air-Sea Interaction, A. Zancala, Editor, pp. 285-291.

13. Norbury, J.R. and White, W.J.K. (1973) Correlation Between Measurements of Rainfall Rate and Microwave Attenuation at 36 GHz, Proceedings of IEE Conference on Propagation of Radio Waves at Frequencies Above 10 GHz, No. 98, London, pp. 45-51.

Generally, the data in Table 2 indicate a decreasing ratio with increasing rain rate. The exception is the JD model which exhibits a slowly increasing ratio with rain rate. This distribution has a large number of small drops compared to the others and referring to Table 1, the attenuation ratio increases with diameter for very small drop diameters. The LP and MP ratios are very similar, which was expected due the similarity of the distributions. The JT distribution ratios are much lower than the other distribution ratios at the higher rain rates where the JT distribution should be valid. The low ratios are due to the relatively large drop sizes inherent in the JT distribution. The maximum ratio is 3.22 for the JT distribution at 0.25 mm/hr while the minimum is 1.68 for the JT distribution at 100 mm/hr.

The use of the JT distribution at the very low rain rates is not appropriate since it is a convective rain model associated with much higher rain rates. Discarding the low rain-rate JT values, the LP ratio is highest at 2.82 with the MP value close at 2.79; both occurring at a rain rate of 0.25 mm/hr. Noting that the JT distribution resulted in the lowest ratios, the 150 mm/hr ratio was calculated using the JT parameter values. 150 mm/hr can be considered the most extreme rain rate to be expected under normal circumstances and the JT ratio was 1.64 at that rain rate.

An interesting comparison between the Medhurst constant-diameter ratios and the standard dropsize distribution ratios is the minimum ratio value found in each case. There is a considerable difference between the ratio of 1.64 obtained with the JT distribution at 150 mm/hr and the ratio of 0.98 obtained with 0.65 cm diameter drops. This is a result of there being relatively few large diameter drops in rain, even at very high rain rates. For example, looking at the Laws and Parsons distribution as tabulated by Medhurst, [5] only 12.2 percent of the total volume at a rain rate of 100 mm/hr has a diameter greater than 0.4 cm. The maximum ratios, on the other hand, agree fairly well with 2.94 for constant-diameter drops and 2.82 for the LP distribution.

The last comparison to be made is the dependence of the ratio on temperature. Normally, the $0^{\circ}C$ value is most appropriate for temperate climates while the $20^{\circ}C$ and $-10^{\circ}C$ data are useful as boundary values. In addition, the $-10^{\circ}C$ values are applicable when considering supercooled rain which has been found to be not an uncommon occurrence. Table 3 lists the attenuation ratios for five rain rates and three temperatures for the four dropsize distributions considered in Table 2. The first fact evident from Table 3 is the non-uniformity of the effect of temperature. For the LP and MP distribution, the ratio decreases with increasing rain rate and decreasing temperature for rain rates below 10 mm/hr; above 10 mm/hr, the ratio increases with decreasing temperature. The JT distribution results in increasing ratio with decreasing temperature up to 100 mm/hr where again the inverse occurs, although weakly. The JD distribution, at the rain rates where it

Table 3. Temperature Dependence of Attenuation Ratio as a Function of Rain Rate and Dropsize Distribution

LP Distribution						
Rain Rate (mm/hr)	1	5	10	50	100	
Temperature (^{o}C)						
+20	2.76	2.42	2.29	1.89	1.78	
0.0	2.60	2.38	2.29	2.05	1.90	
-10	2.54	2.36	2.28	2.04	1.88	
MP Distribution						
Rain Rate (mm/hr)	1	5	10	50	100	
Temperature (^{o}C)						
+20	2.83	2.48	2.35	2.06	1.95	
0.0	2.60	2.41	2.32	2.15	2.08	
-10	2.52	2.37	2.30	2.16	2.10	
JT Distribution						
Rain Rate (mm/hr)	1	5	10	50	100	150
Temperature (^{o}C)						
+20	2.55	2.21	2.09	1.81	1.70	1.64
0.0	2.77	2.33	2.16	1.81	1.68	1.61
-10	2.92	2.41	2.22	1.83	1.69	1.61
JD Distribution						
Rain Rate (mm/hr)	1	5	10	50		
Temperature (^{o}C)						
+20	2.72	2.70	2.20	2.68		
0.0	2.44	2.55	2.59	2.72		
-10	2.34	2.46	2.51	2.64		

is appropriate to use it, results in a decreasing ratio with decreasing temperature. This is also true at a rain rate of 0.25 mm/hr, although it is not shown in the table.

Thus far, all of the discussion on theoretical attenuation ratios has actually considered only specific attenuation, that is, the signal attenuation caused by a uniform rain-filled space 1 kilometer in extent. At this point, consideration of attenuation ratios along an earth-to-space path is appropriate. Two approaches, of the many published, concerning development of rainfall distributions along a path were examined. The first, entitled "Synthetic Storm Model", is an empirically derived model which accounts for non-uniform rain rates and seems to fit experimental data from several different locations at several different frequencies.[14] Using the Synthetic Storm calculations as published in several papers, the effective path length for the Prospect Hill location and with an elevation angle suitable for both COMSTAR D-2 and D-3 is 5.95 km. The Synthetic Storm Model splits the effective path into two parts; one part is 1.19 km long and the other is 4.76 km in length. The shorter section has a rain rate always equal to the surface rain rate, while the rain rate in the larger section is

$$RR_{surf} = \begin{cases} R_{surf} & R_{surf} \leq 10 \text{ mm/hr} \\ R_{surf}(R_{surf}/10)^{-0.66} & R_{surf} > 10 \text{ mm/hr} \end{cases} \quad (2)$$

The path attenuation is the sum of the two section attenuations using the applicable specific attenuation for each section. Table 4 contains the total path attenuations at 19.04 GHz and 28.56 GHz and the attenuation ratios for rain rates from 0.25 mm/hr to 100 mm/hr. A Laws and Parsons dropsize distribution with a drop temperature of $0^{\circ}C$ was assumed and the specific attenuations are from Olsen as used in the previous tables. Since the Synthetic Storm Model assumes a homogeneous rain rate for surface rain rates less than 10 mm/hr, the ratios corresponding to rain rates of 10 mm/hr or less are identical to the LP ratios in Table 2. The ratios for rates above 10 mm/hr are slightly larger than the homogeneous case, reflecting the presence of lower rain rates along the path. The path attenuations are included to give an indication of typical attenuations to be expected for the Prospect Hill to COMSTAR D-2 and D-3 paths.

It is well known that the instantaneous correlation between surface rain rate and slant path attenuation is very low. However, by comparing surface rain rate and

14. Persinger, R.R. and Stutzman, W.L. (1978) Millimeter Wave Propagation Modeling of Inhomogeneous Rain Media For Satellite Communication Systems, Virginia Polytechnic Institute and State University, NASA-CR-156817, June.

Table 4. Theoretical Slant Path Attenuations and Ratios of Attenuation at 19.04 GHz and 28.56 GHz as a Function of Rain Rate

Rain Rate (mm/hr)	Attenuation (db)		Persinger Ratio	Hodge Ratio
	19 GHz	28 GHz		
0.25	0.07	0.20	2.82	2.89
0.50	0.15	0.41	2.71	2.68
1.00	0.33	0.86	2.60	2.50
2.00	0.71	1.79	2.50	2.33
5.00	2.00	4.75	2.37	2.12
10.0	4.35	9.92	2.28	1.98
20.0	6.42	14.4	2.24	1.84
50.0	11.7	25.0	2.14	1.67
100.	19.6	39.7	2.02	1.56

Dropside distribution is Laws and Parsons
Temperature is $0^{o}C$
Elevation angle is 36^{o}
Location is New England

slant path attenuation using equal probability of occurrence techniques, a good correlation is possible. Persinger, et al[14] obtained correlation coefficients greater than 0.96 when fitting slant path attenuation to surface rain rate with a power curve and using equal probability of occurrence.

The last column in Table 4 represents attenuation ratios calculated by means of a technique developed by Hodge.[15] Hodge assumed that the rainfall along a slant path was a Gaussian function of position along the path as expressed in Eq. (3).

$$R(x) = Ro\ e^{(-(x/Lo)^2)} \tag{3}$$

where

Lo = measure of sample extent

x = position on path

Ro = peak rainfall rate on path

Using this rainfall rate distribution, Hodge derived an expression giving attenuation ratio as a function of one attenuation and two sets of parameters a1, b1 and a2, b2, where a and b are the constants in Eq. (1). Again using a Laws and Parsons

15. Hodge, D.B. (1977) Frequency scaling of rain attenuation, IEEE Transactions on Antennas and Propagation, AP-25, pp. 446-447.

dropsize distribution and assuming a drop temperature of $0^{\circ}C$, the following expression for the ratio of 28.56-GHz slant path attenuation to 19.04-GHz slant path attenuation results

$$A28/A19 = 2.367\ (A19)^{-0.0509} \qquad (4)$$

where

A19 = 19.04 GHz attenuation (db)

A28 = 28.56 GHz attenuation (db)

The ratios in Table 4 using Eq. (4) were calculated using the corresponding 19.04-GHz slant path attenuation from the Synthetic Storm Model. The two sets of ratios are in close agreement considering the different approaches taken in developing the techniques to calculate them.

The phase dispersion due to rain along a communication link has received little attention in past publications. The best explanation of the lack of attention is the small magnitude of phase dispersion expected and therefore the inconsequential effect on microwave systems. Crane[16] examined coherent pulse transmission through rain and concluded that for carrier frequencies above 10 GHz, the attenuation along a path had to approach 100 db for significant pulse distortion to occur. Gaussian pulse lengths as short as 0.28 nsec corresponding to bandwidths of over 3 GHz were included in Crane's study. Based upon these numbers, phase dispersion over 1-GHz bandwidths for reasonable path rain rates, should not be a problem for typical communication links.

Oguchi[17] and Chu[18] have presented the results of scattering calculations giving specific attenuations and specific phase rotations for several rain rates at different frequencies. Chu's results were selected for use in this report since the two frequencies he used (18.1 GHz and 30.0 GHz) were closer to the experimental frequencies used on the COMSTAR beacons. The phase rotations of Chu were linearly scaled to give a phase dispersion in deg/km for both the 28-GHz sideband case (1056-MHz spacing) and the 19-GHz to 28-GHz carrier phase comparison case. Linear scaling is justified since the real part of the refractive index of water is essentially linear over the 19- to 28-GHz region of the spectrum (see Crane,[16] Figure 2). These two phase dispersions are presented in columns 2 and 3 of Table 5 as a function of rain rate. In order to calculate typical phase dispersions on the

16. Crane, R.K. (1967) Coherent pulse transmission through rain, IEEE Transactions on Antennas and Propagation, AP-15, pp. 252-256.

17. Oguchi, T. (1973) Attenuation and phase rotation of radio waves due to rain: calculations at 19.3 and 34.8 GHz, Radio Science 8:31-38.

18. Chu, T.S. (1974) Rain induced cross-polarization at centimenter and millimeter wavelengths, Bell System Technical Journal 53:1557-1580.

Table 5. Theoretical Phase Dispersion as a Function of Rain Rate for 28-GHz Sidebands with 1.056-GHz Spacing and 19/28 Carrier Comparison

Rain Rate (mm/hr)	1-GHz Sideband (deg/km)	19/28 Carrier (deg/km)	1-GHz Sideband (deg)	19/28 Carrier (deg)
12.5	0.119	1.13	0.7	6.8
25.0	0.941	8.96	1.7	16.0
50.0	1.345	12.80	5.9	34.3
100.0	1.893	18.0	6.7	64.1
150.0	2.142	19.44	6.9	65.8

Prospect Hill/COMSTAR slant path, the Synthetic Storm Model[14] section lengths calculated earlier were utilized. Columns 4 and 5 of Table 5 give the total phase dispersion expected on a 36° elevation angle slant path. Note that the 28 GHz sideband phase dispersion is less than 7° and the 19/28 phase dispersion is less than 70° even for very heavy rain. It is evident that, theoretically, phase dispersion will not be a problem for systems with operating bandwidths of 1 GHz or less.

3. EXPERIMENTAL CONFIGURATION

The COMSTAR propagation experiment included a ground station receiving terminal located at Prospect Hill and two millimeter-wave beacons developed by COMSAT Laboratories mounted on synchronous orbit satellites owned and operated by COMSAT General Corporation. The two satellite beacons used during the year the ground station was operable were on satellites designated D-2 and D-3 which were located at 95° and 90° west longitude respectively. The closeness of the orbital locations results in only a small change in elevation and azimuth angles when the changeover to D-3, prompted by the shutdown of D-2, occurred. Table 6 lists several parameters of the beacons which are applicable to this experiment. The 19.04-GHz and 28.56-GHz carriers and the 528.8-MHz signal that phase modulated the 28-GHz carrier were derived from a common 132.2-MHz quartz crystal master oscillator. Changes in frequency of the master oscillator were reflected in all three carrier and sideband frequencies. In order to achieve the large dynamic range in received signal level measurement required for the experimental program, the receiver bandwidth had to be very narrow and the spectral properties of the beacon had to have corresponding narrow linewidths. The transmitted signals from the beacon were such that 90 percent of the transmitted carrier power was in a bandwidth of less than 15 Hz at 19 GHz and less than 20 Hz at 28 GHz. The 19-GHz

Table 6. COMSTAR Satellite Beacon Parameters

Station-Keeping Tolerance	<+/- 0.1° E-W and N-S
Antenna-Pointing Tolerance	<+/- 0.1°
Carrier Frequencies	19.0400 GHz and 28.5600 GHz
Variation: Diurnal	<+/- 1 ppm
Aging	<+/- 1 ppm per year
Effective Radiated Power	
19 GHz	>+52 dbm per polarization
28 GHz	>+56 dbm
Variation: Diurnal	<+/- 0.3 db
Aging	<+/- 0.5 db per year
Maximum Rate	<+/- 0.1 db per minute
Phase Modulation (28 GHz Only)	Coherent with Carrier
Frequency	264.4 MHz (D-2), 528.8 MHz (D-3)
Sideband Level	<7db below carrier

channel was polarization-switched at 1000 Hz between a nominally vertical polarization and horizontal polarization at the Holmdel, New Jersey receiving site. Due to changing orbit position assignments prior to launch, the actual received polarization orientation was 21° at Holmdel. The switched-polarization capability of the beacons was not utilized in this experiment.

The receiving site at Prospect Hill consisted of a two-channel phase lock receiver mounted in an 18-foot precision dish which in turn was mounted on an elevation over azimuth angenna mount. A microprocessor-controlled data recording system stored the received signal data on magnetic tape along with certain meteorological data. A desk top calculator provided the pointing angle data to accurately track the satellite position in open-loop fashion. Figure 1 is an overall block diagram of the receiving site.

The two-channel receiver design was unique in order to accurately measure the two carrier signal levels, the two 28-GHz sideband levels, the relative phase of each sideband to the 28-GHz carrier and the relative phase of the 19 GHz carrier to the 28-GHz carrier. Figure 2 is a block diagram of the receiver design and shows the technique developed to meet the above requirements while tracking a slowly changing beacon master oscillator frequency. Figure 3 provides more detail of the phase lock loop portion of the receiver design. The unique part of the design was the frequency shifter which changed the 5.00 MHz of the standard

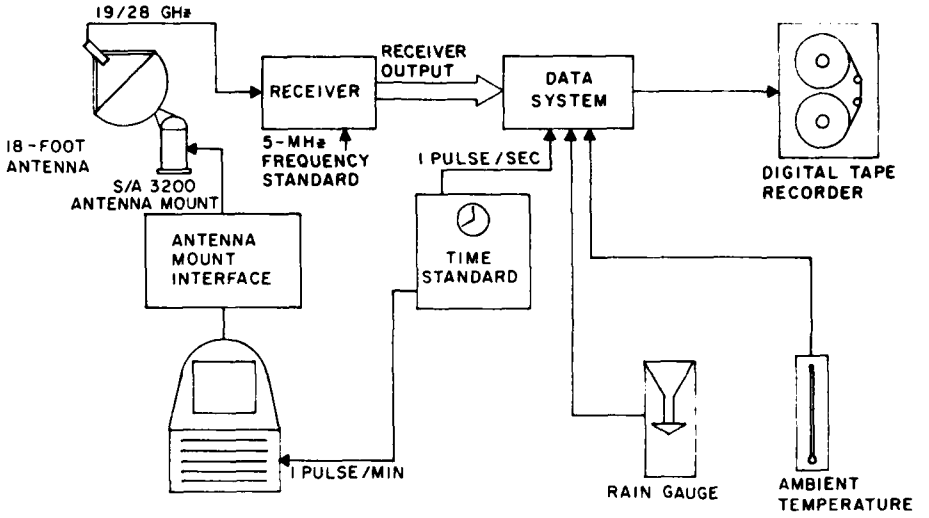

Figure 1. Prospect Hill/COMSTAR Ground Station

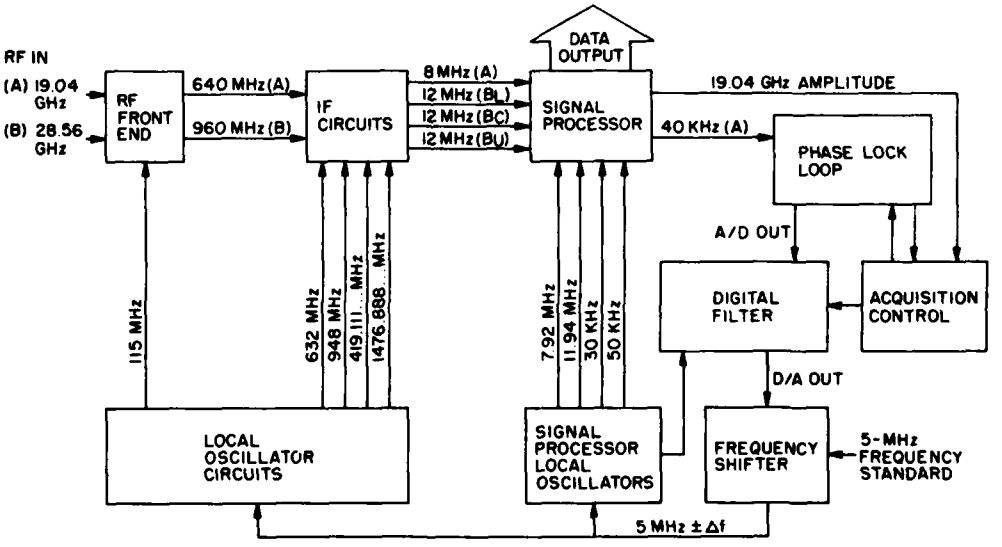

Figure 2. Two-Channel Phase Lock Receiver

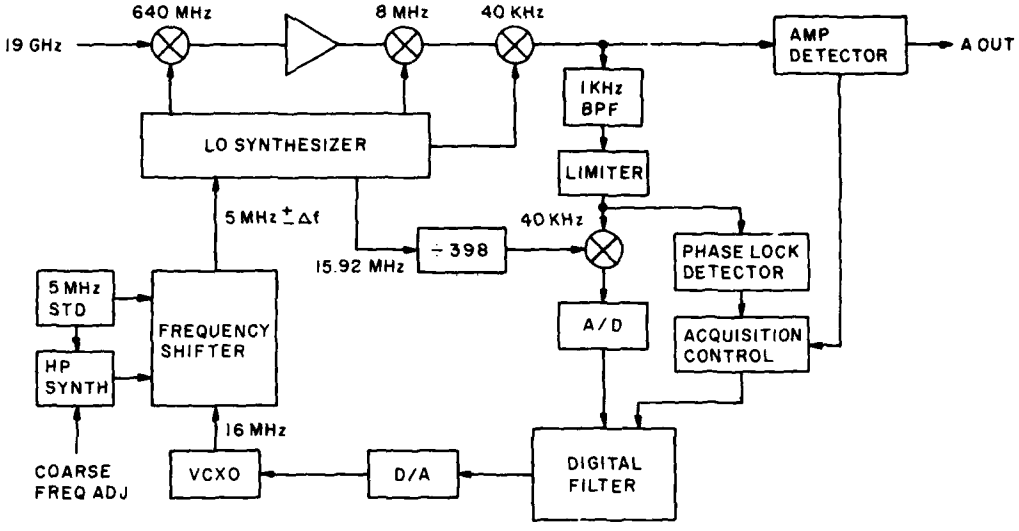

Figure 3. Receiver Phase Locked Loop

oscillator by very small amounts while maintaining the spectral purity of the frequency standard. Spectral purity was required since the final receiver bandwidths were 10 Hz at 19 GHz and 15 Hz at 28 GHz and the local oscillators had to be clean enough to support these narrow bandwidths. The frequency shifted 5.00 MHz was used to synthesize each local oscillator and the amount the 5.00 MHz frequency changed was controlled by the phase lock loop. This ensured that phase coherence was maintained throughout the receiver and allowed phase locking on the 19-GHz carrier to cause the other carrier and sidebands to be accurately tracked. The original receiver design contained logic to prevent the receiver from locking on one of the 19-GHz carrier sidebands that were generated by the 1000-Hz polarization switching. Under normal conditions, the received 19-GHz signal appeared to be a 1000-Hz square wave modulated carrier with its associated frequency spectrum of sidebands spaced at 1000 Hz intervals away from the carrier. Simply sweeping the receiver frequency until lock occurred would result in locking on one of the sidebands instead of the carrier. The original receiver design contained logic to look at the two apparent sidebands about the locked signal to see if their amplitude was less than the carrier. If the levels were not below the carrier, the receiver was forced to sweep until the next signal was locked and the test made again. Eventually, this should have resulted in locking to the carrier, however, in practice the logic did not always work and the process of locking onto the correct

signal was a manual one. This led to the loss of some data when the system broke lock during periods when the site was unattended.

The antenna system consisted of an existing 18-foot parabolic reflector and commercial mount. The antenna had been designed to work at 22 GHz and previous pattern tests at 35 GHz indicated that it would be more than adequate at 28 GHz for the purposes of this experiment. The antenna was a prime focus type and the receiver front end and the diplexer/feed horn were mounted in a 12-inch diameter tube, 3 feet long which was anchored at the proper position. Antenna patterns were measured using the beacon signals and the position of the antenna feed horn was adjusted for the best pattern. The final feed position was a compromise between the best position for each frequency. The final antenna beamwidths were 0.22° at 19 GHz and 0.18° at 28 GHz with first sidelobes being 20 db below the peak. The 19 GHz beamwidths were in good agreement with theoretical values while the 28 GHz beamwidths were larger than expected due to under-illumination of the reflector, which was in turn due to the use of a common feed horn for both frequencies. The primary feed horn patterns were not the same at the two frequencies and the horn design was a compromise between efficiency and beamwidth. Antenna gain was not measured with the satellite beacon feed assembly installed.

The antenna mount was a Scientific Atlanta type 3200 with an unusual drive system. The standard drive for this mount was a servo-type system capable of high tracking and slewing rates. This particular mount was delivered with a stepper motor drive with direct coupling from the stepper to each axis through specially selected gear boxes with very low backlash. Each step of the stepper drive resulted in a 0.0025° movement of the mount and position accuracy checks using an auto-collimeter indicated accuracies of 0.01° were readily achievable. The main disadvantages to the stepper drive were slow slewing of about 20° per minute and a finite load capability in terms of torque capability. The slow slewing was no problem for tracking the beacons since their position changes were very small and very slow. The torque limitation was more serious because strong gusty winds and occasional snow and ice loading were enough to cause the steppers to lose "lock". Stepper motors have a property that when their holding torque is exceeded, the motor "breaks loose" and the holding torque falls to near zero until rotation ceases. Whenever a wind gust sufficiently strong occurred to exceed the stepper motor holding torque, the antenna would swing 90 to 180° and of course the beacon signal would be lost. Usually this would happen in the middle of a rainstorm while the site was unattended and attenuation data would again be lost. The final destruction of the antenna occurred when an ice load built up in the antenna and the holding torque was exceeded. Unfortunately, when the torque was exceeded, the antenna descended at a rapid rate and was destroyed when it hit the roof of the building.

The control of the pointing commands for the antenna was by means of a Wang 1200 calculator with an external interface allowing the antenna commands to be output to the mount and time information to be input to the calculator. The COMSTAR Satellite, like all geosynchronous orbit satellites, appeared to be stationary to an observer on Earth. However, the COMSTAR orbit was precisely controlled so that the apparent elevation and azimuth would not vary more than 0.10°. This allowed fixed pointing for small antennas or for larger antennas in cases where a slight variation in signal level was allowable. With the beamwidths of the 18-foot antenna, the 24-hour variations were about 2 db which was considered to be unacceptable. Slabinski[19] found that for satellites with station-keeping capability similar to COMSTAR, the apparent elevation and azimuth could be calculated from expressions of the form of Eq. (5) with errors less than 0.008° over a 14-day period.

$$POS = Co + C1\ t + C2^2\ t + (Cc1 + Cc2\ t) \cos W + (Cs1 + Cs2\ t) \sin W \qquad (5)$$

where

POS = azimuth or elevation angle
t = time in days since some epoch date
W = 6.3003881 t

The constants C0, C1, C2, Cc1, Cc2, Cs1, and Cs2 are derived from a numerical curve-fitting process to the satellite position over a 7-day period. The constants were good for a 14-day period if no satellite station-keeping maneuvers were carried out. As a rule, new constants were calculated and distributed every 7 days to each station using them. The pointing accuracy using the above approach at Prospect Hill was less than 0.01° whenever current constants were used.

The Wang calculator was used to calculate Eq. (5) for each axis, once per minute, and the resulting positions transferred to the antenna mount interface. The calculator derived time by using a once-per-minute interrupt from the station time standard, and then incremented time from a set time entered via the calculator keyboard. The new weekly constants were also entered via the keyboard. Positions were calculated to 0.001° and the once-per-minute update was more than adequate for this purpose. The two positions, each consisting of 6 BCD characters, were transmitted to an interface unit which supplied the stepping commands to the antenna mount. The interface unit kept track of the antenna position relative to a known position by incrementing or decrementing a counter as pulses in the two

19. Slabinski, V.J. (1975) Expression for the time-varying topocentric direction of a geostationary satellite, COMSAT Technical Review 5:1-14.

directions were sent to the stepper motors. Conversion between step count and actual position in degrees was accomplished by the interface. As the commanded position changed, the interface would output pulses to move the antenna to the required position. As long as the antenna moved one pulse position for each supplied pulse, tracking was accurate to 0.01° or better. As mentioned before, high wind gusts would eliminate the one-to-one position to count correspondence and the mount/interface would have to be renormalized at the reference position. The wind gust problem was in the process of being solved by adding another gear reduction in series with the stepper motors when the antenna failure occurred.

The final hardware associated with the ground site was the data recording system. This unit consisted of a 9-track IBM compatible magnetic tape unit, a 16-channel A/D converter, a digital clock and an 8080 microprocessor system. The data recording system stored up to 16 channels of data in memory every 5 seconds and transferred the memory contents to magnetic tape every 2 minutes. Time of day and date were also recorded as a header on the magnetic tape record. The 5-second interval was controlled by signals derived from the station time standard. Table 7 lists the data channels recorded by the data system. Although data was continuously sampled at a once-per-5-second rate, one 2400-foot reel of magnetic tape was sufficient to record data for 28 days.

Table 7. Data System Channels Recorded

1. Time and Date
2. 19 GHz Carrier Level
3. 28 GHz Carrier Level
4. USB (28 GHz) Level
5. LSB (28 GHz) Level
6. USB to Carrier Relative Phase
7. LSB to Carrier Relative Phase
8. 19 GHz Carrier to 28 GHz Carrier Relative Phase
9. Equipment Ambient Temperature
10. Outside Ambient Temperature
11. Tipping Bucket Rainguage Readout

As data collection began, it was soon obvious that an uninterruptible power source for the ground site electronics was a necessity. Several power failures and "line bumps" occurred in the first few months of operation and on each occasion the system would either lose phase lock, lose antenna position reference, shut

down the data system, or all three. A 1500-kva standby supply capable of powering the system for 2 hours was procured and installed. This supply powered all of the electronics of the ground site and eliminated power problems as a cause for loss of data.

The performance of the system met the original experimental requirements except for the reliability. The 19-GHz dynamic range was 35 db and the 28-GHz dynamic range was 42 db. The linearity of the system was measured and the 19 GHz channel was linear to within +/-0.2 db while the 28 GHz channel linearity was +/-0.22 db. The short term carrier level stability was about 0.2 db for both channels and the day-to-day carrier level changes were less than 0.5 db. The relative phase measurements were accurate to within 3^{o} but all three phase channels exhibited a strong dependence on the equipment ambient temperature. This temperature dependence was generally not a problem since the temperature variations were much slower than any measured phase shifts due to rain.

4. DATA ANALYSIS

Although the experiment was designed to provide statistically reliable attenuation data at 19 GHz and 28 GHz, the actual data collection effort did not provide sufficient contiguous coverage of rain events to justify a statistical analysis as performed by Arnold, et al[20] and Harris and Hyde.[21] The system was operating from 1 Jan 78 until 1 Jan 79, but the operation suffered from numerous gaps. The source of these gaps was primarily equipment problems as explained in Section 3. The magnitude of these gaps can be seen in the following discussion. Assuming that 8760 hours of potential data collection existed in 1979, the ground site was not functional for 491 hours or 5.6 percent of the time. Of the remaining 8269 hours, only 290 hours contained significant attenuation events, which were selected for archiving. The normal data-reduction procedure was to read the raw data tape and generate a summary listing giving receiver output values at one-half hour intervals and next, generate line-printer plots of the carrier levels and relative phase shifts. The line-printer plots were 2-minute averages so that attenuation events could be identified easily. Portions of the data tape containing attenuation

---

20. Arnold, H.W., Cox, D.C., Hoffman, H.H., and Leck, R.P. (1979) Rain attenuation statistics from a 19 and 28 GHz COMSTAR beacon propagation experiment: one year cumulative distributions and relationships between two frequencies, IEEE Transactions On Communications, COM-27, pp. 1725-1738.

21. Harris, J.M. and Hyde, G. (1977) Preliminary results of COMSTAR 19/29-GHz beacon measurements at Clarksburg, Maryland, COMSAT Technical Review 7:599-623.

events were archived on a separate magnetic tape for analysis. The criterion for the selection of data for archiving was an attenuation greater than 1 db at 19 GHz. When events were spaced close together in time, the entire period was archived. Therefore, 19-GHz attenuation was not 1 db or greater for the entire 290 hours of archived data. Approximately 61 hours of the archived data were not used for this report because the data were contaminated by ice collecting on the surface of the antenna which resulted in defocusing of the antenna beams or because the 28-GHz beacon on D-2 was off for several days.

The normal rainfall in the Boston area is 42.3 inches and in 1979 the rainfall measured 37.6 inches at the Logan Airport monitoring point. Nackoney[22] measured 38.4 inches at a location approximately one mile from Prospect Hill. The measured rainfall at Prospect Hill was 29.62 inches, but this total did not include frozen precipitation since the rain gauge and collector were not heated. The lack of frozen precipitation data was the difference between Nackoney's total and the Prospect Hill total. The ground site was not functional during 14.5 inches of the Prospect Hill rain-gauge time period. Therefore, attenuation and phase data were collected on only 15.1 inches of rainfall which represents only 39 percent of the total precipitation for the year. Obviously this low percentage did not allow for the generation of availability plots as is normally the case. The lack of contiguous data did not affect the analysis of the ratio of attenuations or the phase dispersion other than limiting the amount of data available.

The attenuation ratio data were calculated by two methods; the first an average of instantaneous samples, and the second a comparison of equal probability of occurrences. The archived data were organized into 19-GHz attenuation bins with bin sizes of 0.5 db for attenuations up to 5.0 db and 1.0 db for attenuations up to 18 db. An upper limit of 18 db was adopted for the 19-GHz data since the corresponding 28-GHz attenuation would be about 35 to 38 db which is the limit of the dynamic range of the receiver. Once the data were organized into 19-GHz attenuation bins, the corresponding 28-GHz attenuations were used to calculate a set of ratios for each bin. The mean ratio, the standard deviation of the ratio, the mean attenuation and the number of samples for each attenuation bin for 29 separate attenuation events were tabulated. The ratio statistics were then calculated for all the attenuation events combined. The combined statistics are presented in Table 8 along with the number of 5-second samples used to calculate the statistics. Since the 19-GHz data were organized into bins, the percent time distribution of the 19-GHz attenuation was available. The 28-GHz attenuation data were organized in

---

22. Nackoney, O.G. (1979) CTS 11.7 GHz Propagation Measurements, Third Year's Data and Final Report, GTE Laboratories Technical Report TR79-471.3, October.

Table 8. Measured Attenuation Ratios as a Function of 19-GHz Attenuation

19-GHz Attenuation (db)	Instantaneous Sample Ratio			Number of Samples	Equal Probability of Occurrence Ratio
	Mean Ratio	Standard Deviation	Mean Attenuation		
1.0-1.5	1.66	0.53	1.18	19803	
1.5-2.0	1.82	0.38	1.68	11220	1.84
2.0-2.5	1.91	0.29	2.17	6335	1.88
2.5-3.0	1.92	0.26	2.68	3.43	1.87
3.0-3.5	1.95	0.23	3.20	1818	1.83
3.5-4.0	2.00	0.21	3.68	1786	1.77
4.0-4.5	2.07	0.23	4.26	1027	1.88
4.5-5.0	2.13	0.22	4.68	750	2.03
5.0-6.0	2.17	0.20	5.40	622	2.20
6.0-7.0	2.19	0.18	6.44	414	2.25
7.0-8.0	2.19	0.18	7.41	321	2.21
8.0-9.0	2.20	0.15	8.44	268	2.22
9.0-10	2.18	0.17	9.47	137	2.22
10-11	2.20	0.17	10.5	103	2.20
11-12	2.15	0.17	11.5	102	2.16
12-13	2.11	0.21	12.4	110	2.17
13-14	2.17	0.17	13.4	71	2.19
14-15	2.14	0.20	14.3	48	2.21
15-16	2.19	0.09	15.5	35	2.20
16-17	2.17	0.08	16.5	36	2.15
17-18	2.11	0.07	17.4	45	2.12

the same fashion except the bin sizes were different. The 28 GHz bins were 1.0 db up to 6 db and 2.0 db up to 38 db. The 19-GHz and 28-GHz percent time distributions are plotted in Figure 4. The lack of large attenuations, due to missing data, is evident in this figure. Scaling Nackoney's[22] 11.17-GHz data for 1978, the total time that the 19-GHz attenuation should have exceeded 10 db was 180 minutes. From Figure 4, the measured time for attenuations greater than 10 db was 46 minutes. By comparing attenuations with the same probability of occurrence, a "smoothed" attenuation ratio can be calculated. This ratio is also listed in Table 8. The two sets of ratios are close in value over the attenuation range measured.

The first and most obvious fact evident in Table 8 is the ratio variation with attenuation. Although the theoretical ratios varied depending upon methods and models used, they all had decreasing ratios with rain rate or attenuation. The

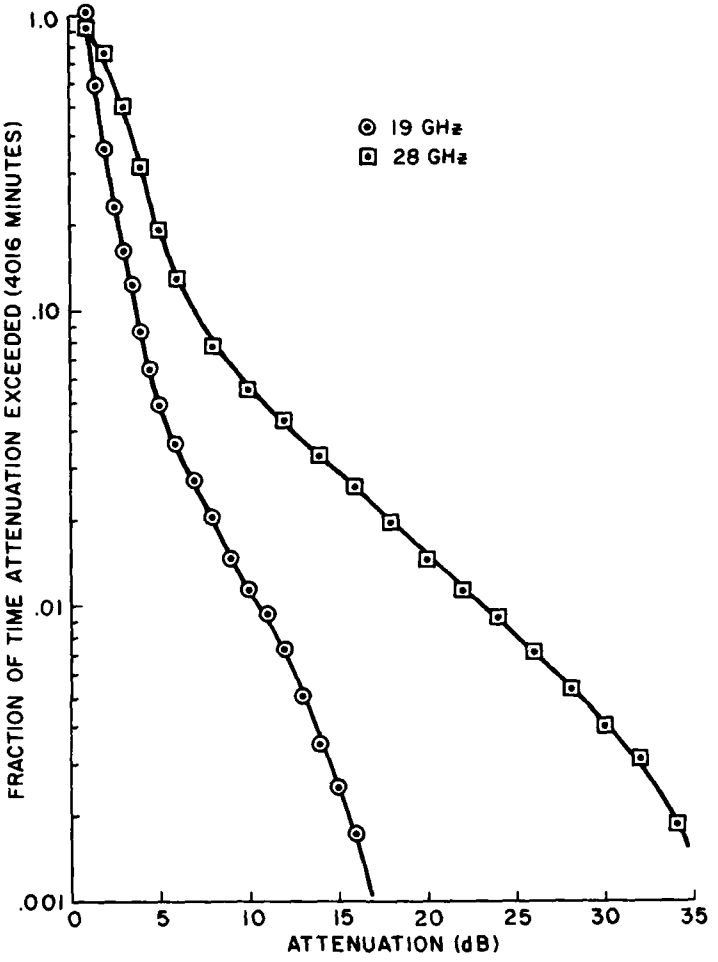

Figure 4. Cumulative Distribution of 19-GHz and 28-GHz Attenuation

ratios in Table 8 first increased with attenuation, peak at about 7 db of attenuation at 19 GHz and then slowly decrease. Figure 5 illustrates this more clearly and also contains the Persinger and Hodge ratios as listed in Table 4. The other interesting feature in Figure 5 is the standard deviation values of the instantaneous ratios. The spread in the lower values is relatively large, indicating the variability in raindrop distributions that occur at low rain rates. Previous experimenters have found a large variation in attenuation ratio on a rain-event-to-rain-event basis[1, 4] and the same was true in the data collected at Prospect Hill. Figure 6

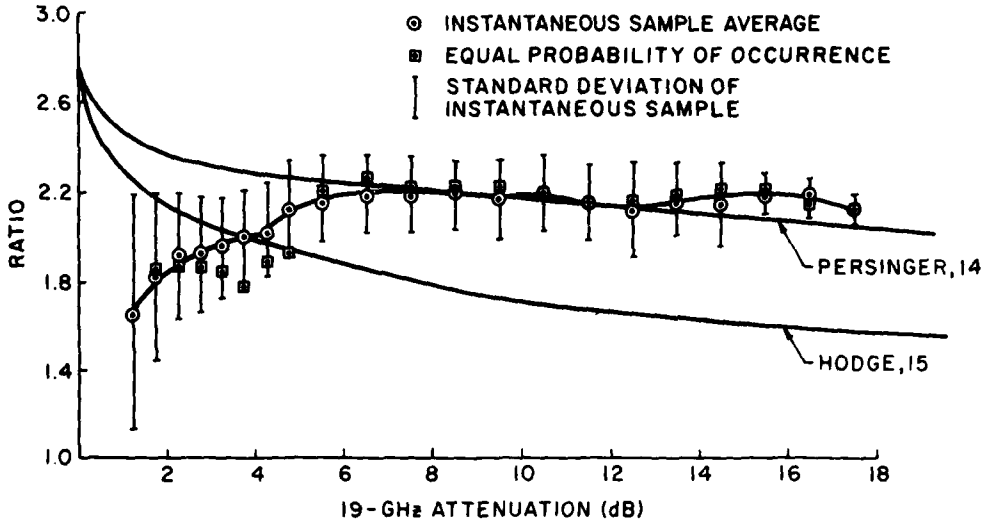

Figure 5. Attenuation Ratio vs 19-GHz Attenuation, Model Data and Measured Data

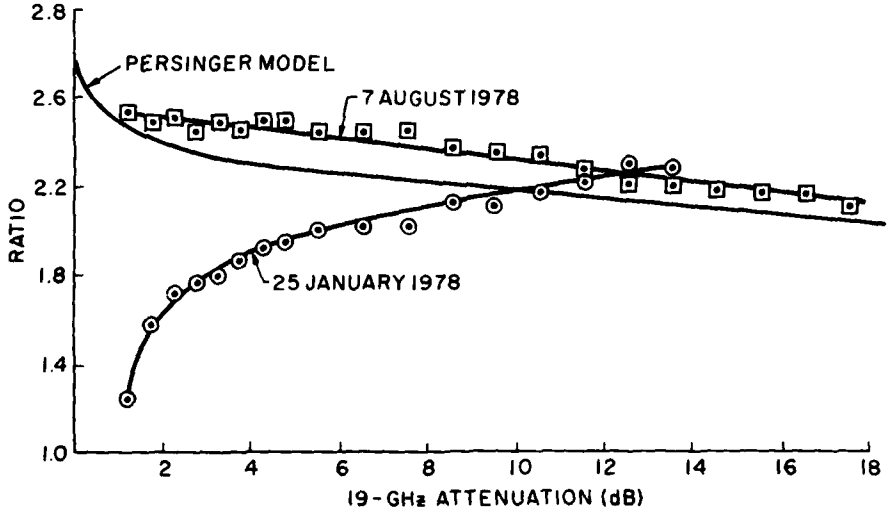

Figure 6. Variations In Attenuation Ratio vs 19-GHz Attenuation

contains two curves representing the largest, and the smallest ratios observed. All of the data seem to converge on a ratio between 2.1 and 2.2 for attenuations greater than 10 to 12 db which is in good agreement with the Holmdel, New Jersey data of Arnold, et al.[20] Three sets of data from locations in the southern part of the country had attenuation ratios which were closer to 1.8 for 19-GHz attenuations greater than 10 db.[23, 24, 25] The occurrence of low ratios at low attenuations is not as rare as a casual scan of the literature would suggest. Most published ratio data were calculated using the equal probability of occurrence technique which eliminated the scatter that would appear if the instantaneous sample technique was used. Figure 7(a) of Hogg and Chu[1] contains 30.9 GHz/18.3 GHz instantaneous ratio data from a 2.6-km terrestrial link. The ratios vary from less than 1.0 to over 5.0 for low attenuations and the spread is attributed to storms with special dropsize distributions. Attenuation ratio data from ATS-6 at 20 GHz and 30 GHz were reported by Ippolito.[4] The spread in the 30 GHz/20 GHz instantaneous ratio was from under 1.0 to over 4.0. In this case, even the equal probability of occurrence ratios had relatively large variations of from 1.3 to over 2.0 although the data sample was small. The several plots of the instantaneous 35 GHz/15 GHz ratios included in Altshuler and Telford[10] also have large ratio spreads for the low attenuations. The variability of the ratio at low attenuations is common, the low ratios obtained when using the equal probability technique is less common.

The comparison of the measured data to the theoretical models presented a problem, primarily because of the low ratios at the low attenuations. Referring to Figure 5, the Persinger model provides a remarkable fit for 19-GHz attenuations above 6 db. The August rain event shown in Figure 6 is also in good agreement with the Persinger model, even for the low attenuations. The low ratios for low attenuations as illustrated by the January event in Figure 6 and the average data in Figure 5 implies a larger dropsize for the lower rain rates than most of the dropsize distributions predict. The low ratios at low attenuations were also prevalent in 35-GHz to 15-GHz attenuation ratio data reported by Altshuler and Telford[10] and measured at the same location. Comparing the measured data with the individual dropsize distribution results given earlier in Table 2, the Marshall-Palmer distribution has the best fit for 19-GHz attenuations above 6 db, although, again the low attenuation Marshall-Palmer ratios are much higher than measured.

---

23. Bergmann, H.J. (1978) A mm-Wave Propagation Experiment in Georgia and Illinois Utilizing COMSTAR Beacon Signals, USNC/URSI Meeting, University of Maryland, May.

24. Tseng, F. and Hyde, G. (1978) Frequency scaling of attenuation above 10-GHz, EASCON, pp. 396-403.

25. Bloch, S.C., Davidson, D., and Tang, D.D. (1978) Rain-attenuation experience with the Tampa triad using 19 GHz COMSTAR satellite beacon signals, EASCON, pp. 379-384.

The measurement of phase dispersion using the COMSTAR beacons was not as straightforward as the attenuation measurements. The expected sideband phase change was close to the receiver phase resolution and the receiver relative phase output was a strong function of equipment ambient temperature. The narrowband filters used to achieve the 15-Hz bandwidths at 28 GHz were identified as being the most likely cause for the temperature sensitivity. In any case, the room temperature was normally stable except for air conditioner transients and the temperature effects could either be ignored or removed. The original beacon design had the 19-GHz and 28-GHz antennas co-located so that a 19-GHz to 28-GHz phase comparison could be made. The final design resulted in the two antennas being separated by the width of the spacecraft, about 8 feet.

Since the spacecraft was spin-stabilized with the antenna platform fixed, the antenna pointing had a wobble with approximately a 1-second period corresponding to the spin rate. The wobble causes the phase centers of the beacon antennas to move which changes the received phase between the two carriers. The net effect of these problems was to make quantitative measurements of small phase changes impossible; however, some information was derived from selected events when the temperature variation of the equipment was gradual and when the spacecraft pointing was relatively stable. One other limitation to the phase data was the dynamic range of the phase determination hardware in terms of 28-GHz signal level. Tests of the receiver phase system linearity indicated no errors as a function of signal level, however as the signal to noise decreased, the phase outputs became noisy for 28-GHz attenuations exceeding about 28 db. Above that level, the phase outputs were stable while below that level, the outputs had instabilities not related to the received phase.

With all these restrictions in mind, three events were selected for inclusion in this report. All three occurred when the D-3 beacons were being observed since the sideband spacing on D-3 was 1056 MHz compared to the 528-MHz spacing on D-2. The temperature sensitivity of the receiver seemed to be less with the wide sideband filters installed and the wide spacing enhanced the measured phase shift. The three events were on 17 September 1978 (day 260), 6 October 1978 (day 279) and 14 October 1978 (day 287). Three figures are presented for each day; each figure includes a time plot of the 28-GHz signal level as well as one of the three phase outputs from the receiver. Day 260 had one clean fade event with a fade depth of 26 db at 28 GHz. Figures 7 and 8 contain the upper side-band-to-carrier phase and the lower sideband-to-carrier phase respectively. In both cases, the non-event phase variation is relatively smooth and small. By fitting a curve to the data to represent the phase variation without the event, phase changes of 3^{o} and 4^{o} respectively are measured as expected. The 19/29 phase variations due to the spacecraft were relatively small during day 260 and the phase changes shown in Figure 9

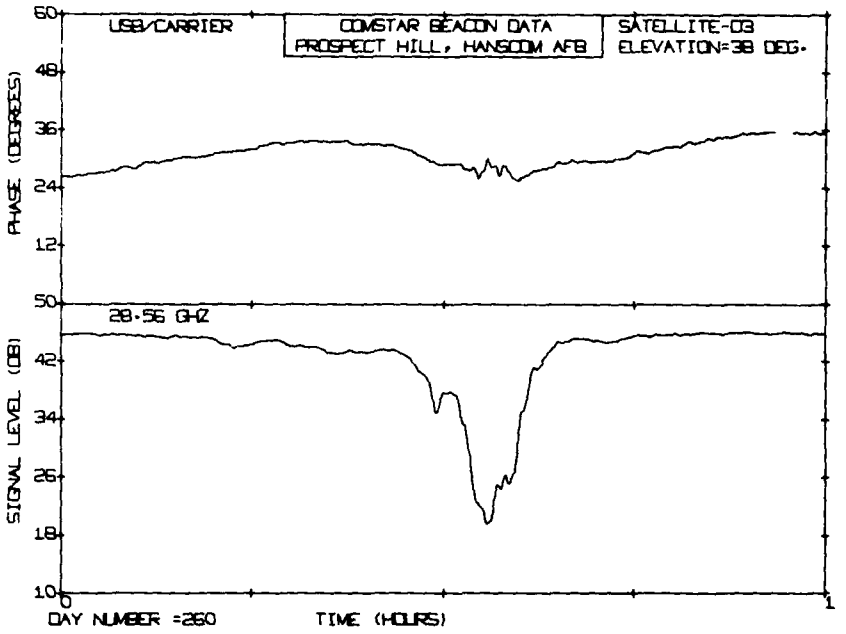

Figure 7. Upper Sideband to Carrier Relative Phase, 17 September 1978

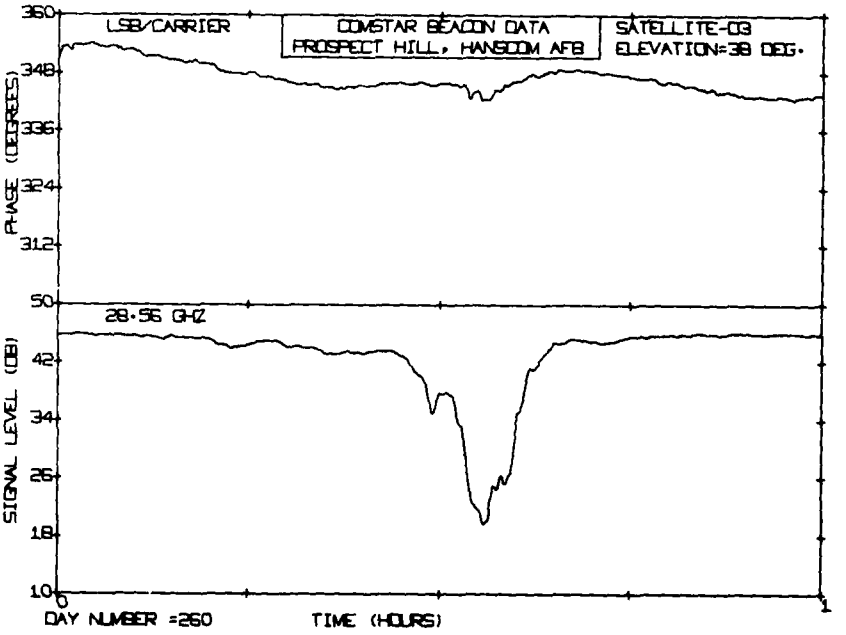

Figure 8. Lower Sideband to Carrier Relative Phase, 17 September 1978

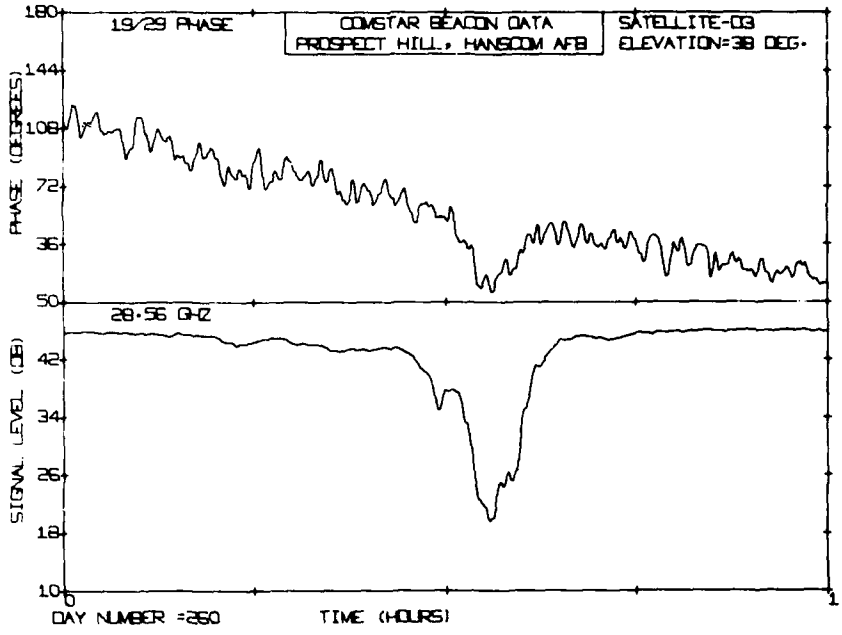

Figure 9. 19-GHz Carrier to 28-GHz Carrier Relative Phase, 17 September 1978

due to the rain event are evident. Again, by fitting a curve to the non-event phase variations and subtracting this from the peak change during the rain event, a phase change of 42^{o} was found. If the phase dispersion was linear with frequency, a 42^{o} change in the 19/28 comparison should correspond to a 5^{o} change across the 28-GHz sidebands which compares well with the total change of 7^{o} measured. Referring to Table 5, a comparison of the measured and theoretical phase dispersion can be made. Using the peak 28-GHz attenuation of 26 db and the Persinger model data in Table 4 to find the apparent surface rain rate of 50 mm/hr, a theoretical 19/28 phase dispersion of 34^{o} would be expected. Considering the measurement difficulties and assumptions made in the theory, the comparison with the measured value of 42^{o} is quite good. The corresponding theoretical phase dispersion across the sidebands is 6^{o} which also compares very well with the data. The analysis of the data recorded on day 279 presented more of a challenge. As shown in Figures 10, 11 and 12, three distinct attenuation events can be identified with attenuations of 9 db, 16 db and 25 db. The upper and lower sideband phase changes are difficult to separate from the temperature effects in the first two smaller attenuation events and the phase data during the larger attenuation is not consistent. The largest sideband phase changes during the larger attenuation event do not correspond with the peak attenuation. The individual phase change peaks in the sideband phase data

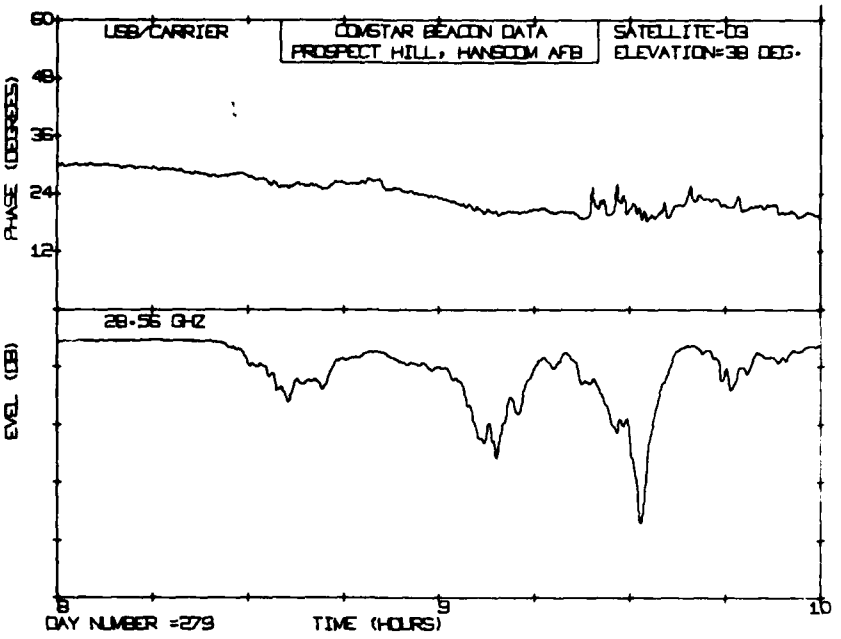

Figure 10. Upper Sideband to Carrier Relative Phase, 6 October 1978

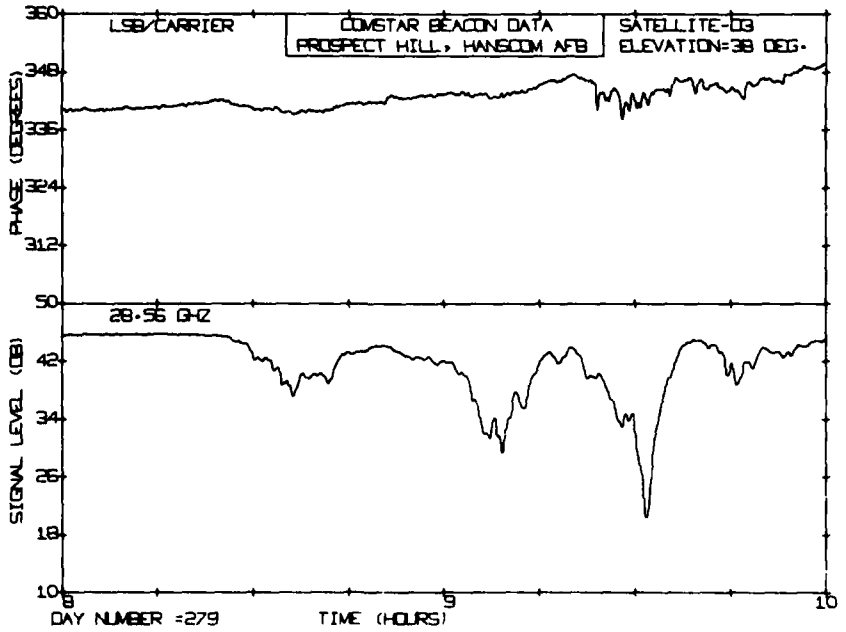

Figure 11. Lower Sideband to Carrier Relative Phase, 6 October 1978

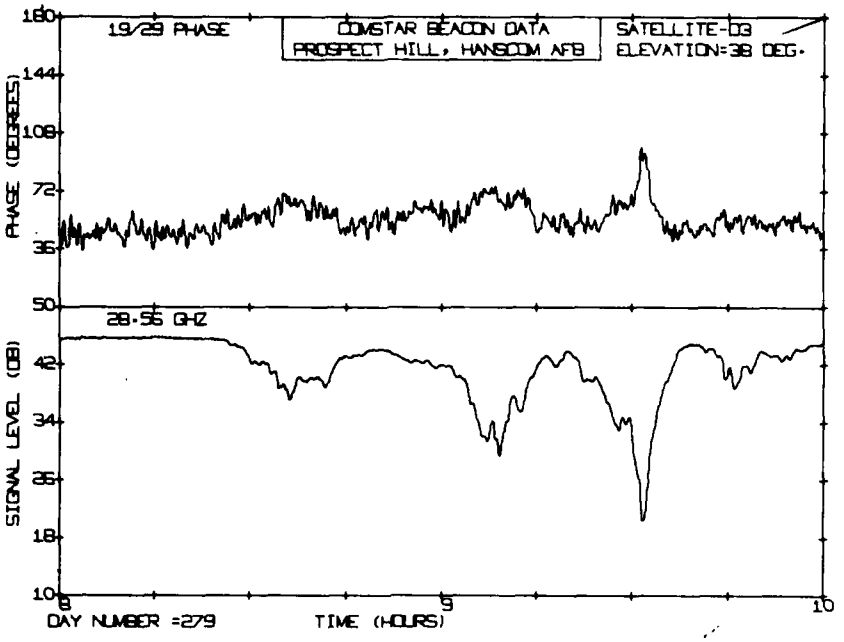

Figure 12. 19-GHz Carrier to 28-GHz Carrier Relative Phase, 6 October 1978

are well correlated in time but not with the attenuation. The 19/29 phase comparison shown in Figure 12 is a littler more consistent. The relative phase change for each of the two smaller attenuation events is about 12^{o} after smoothing the short term variations. The large attenuation phase change is 49^{o}. Comparing the large attenuation phase data with day 260, the 19/29 changes are in good agreement, 49^{o} compared to 42^{o} for a 25-db attenuation and a 26-db attenuation respectively. The theoretical 19/29 phase dispersion of 34^{o} as calculated previously is in fair agreement with the measured data. No usable information can be derived from the sideband phase data, other than the existence of a possible anomalous phase dispersion which is small in any case. The last phase change data is on day 287 which had a simple 18 db fade at 28 GHz. The total sideband phase change derived from Figures 13 and 14 was 5^{o} while the 19/28 phase change shown in Figure 15 was 32^{o}. Using the 18-db fade depth and the assumptions described above, the theoretical 19/28 phase change would be 16^{o}. The measured 32^{o} could be in doubt since the fade duration is long and the accuracy of the baseline curve that was assumed to be the phase variation without attenuation is somewhat uncertain. Assuming phase dispersion linearity with frequency, the sideband phase shift corresponding to the 32^{o} 19/28 change would be 4^{o} which is in good comparison with the measured 5^{o}.

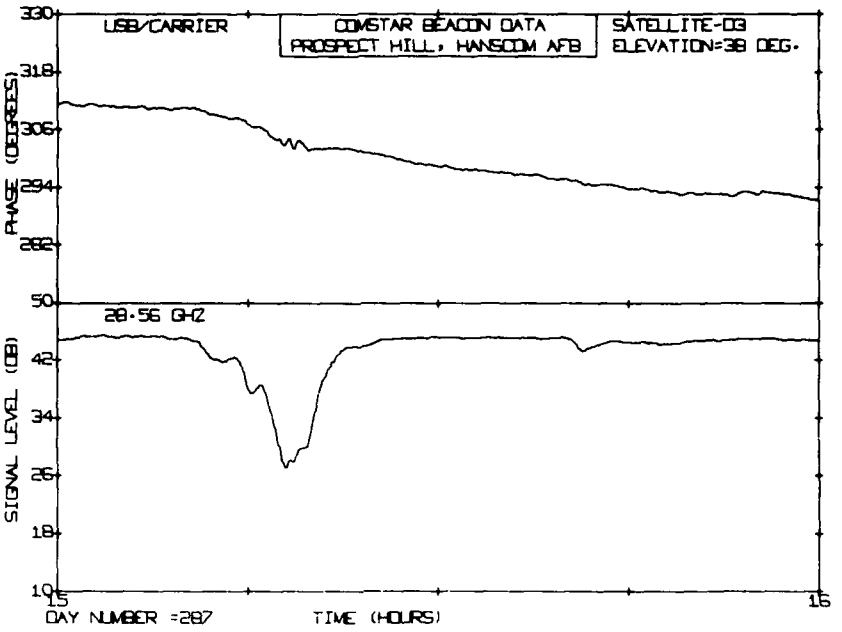

Figure 13. Upper Sideband to Carrier Relative Phase, 14 October 1978

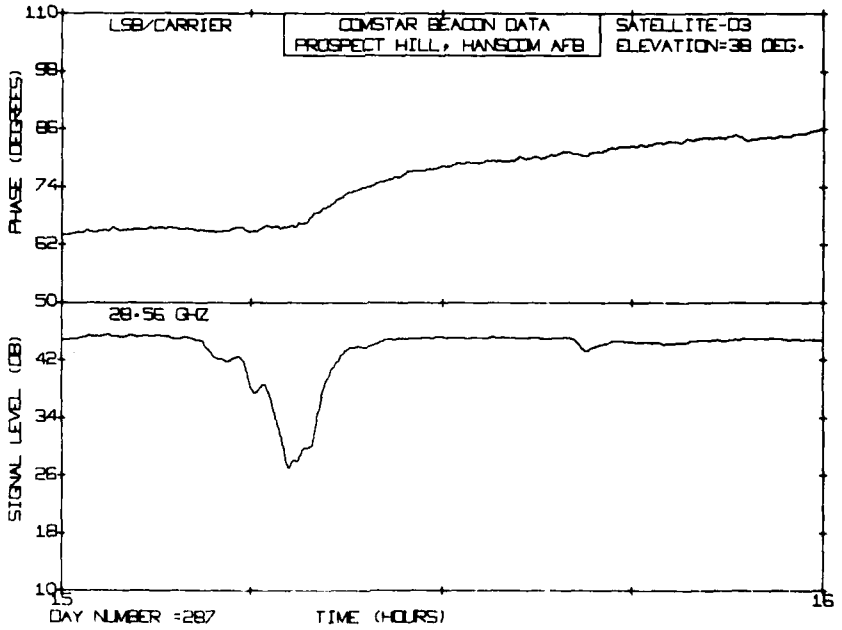

Figure 14. Lower Sideband to Carrier Relative Phase, 14 October 1978

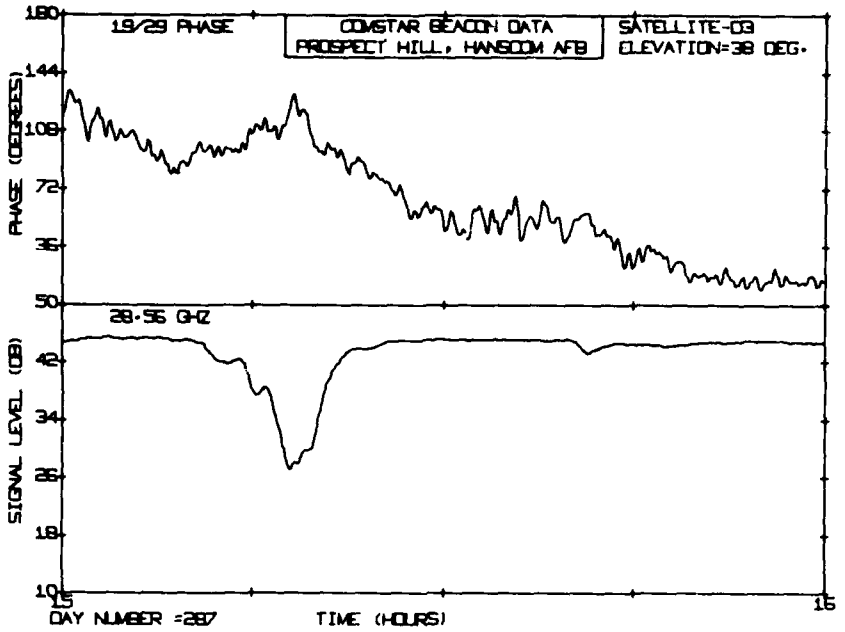

Figure 15. 19-GHz Carrier to 28-GHz Carrier Relative Phase, 14 October 1978

The measured phase dispersion across the 1-GHz sideband spacing was essentially negligible as was predicted by the theory. The 19/28 phase dispersion was at least comparable to the theoretical predictions and is perhaps only of academic interest in any case.

5. CONCLUSIONS

The intent of this report was to discuss the theoretical aspects of attenuation ratio and phase dispersion due to precipitation and to present experimental data to compare with theory. The attenuation ratio concept will be useful as a tool to improve the engineering design of earth-to-space communication links at millimeter wavelengths. Several different theoretical approaches were described and the corresponding expected ratios listed. The comparison of the Prospect Hill experimental ratio data to the theory produced discrepancies. The Persinger model had the best agreement with the experimental ratio data for 19-GHz attenuations greater than 6 db, however, none of the theoretical results compared well with the low attenuation data. The best explanation for the large discrepance is that none of the accepted dropsize models represent the actual rain along a slant path in New England

during periods of light rain. A possible explanation for this discrepancy is that the attenuation is produced by a distribution of widely dispersed large drops as mentioned in of Altshuler and Telford.[10]

Similar results have been found by other investigators as was discussed in Section 4. In addition, the variation in ratio, particularly at low 19-GHz attenuations, was larger than originally expected, although careful review of the literature produced other examples of large variations. The large attenuation ratio seems to be geography dependent with the ratio being lower in the southeastern United States than in the north. The attenuation ratio concept may be useful for calculating attenuations at other millimeter wavelengths, but the limitations as demonstrated in Section 4 have to be kept in mind. For an arbitrary location, the low attenuation ratios in particular have to be suspect while the high attenuation ratios are useful within the geographical variations expected.

The phase dispersion question will finally be answered after all of the COMSTAR beacon data collected by several experimenters are analyzed and published. No serious dispersion was ever expected, particularly over bandwidths of 1 GHz or less. Both the theory and the experimental data show that the 1-GHz phase dispersion will not be a problem for future digital communication systems. The attenuation along a slant path has to be larger than 20 db before measurable phase dispersion appears and at that attenuation level, operational systems will be more adversely affected by the attenuation than the phase dispersion. The phase dispersions measured across the 9.5 GHz between the two beacon carriers could be of concern to some future, ultra-wideband, system; however, high attenuation will cause system problems before phase dispersion does.

References

1. Hogg, D.C. and Chu, T. (1975) The role of rain in satellite communications, Proceedings of IEEE 63:1308-1331.
2. Ippolito, L.J. (1970) Millimeter-Wave Propagation Experiments Utilizing the ATS-5 Satellite, NASA Publication X-751-70-428, Goddard Space Flight Center.
3. Ippolito, L.J. (1972) Earth-Satellite Propagation Above 10 GHz, NASA Publication X-751-72-208, Goddard Space Flight Center, May.
4. Ippolito, L.J. (1976) 20- and 30-GHz Millimeter Wave Experiments With the ATS-6 Satellite, NASA Technical Note #D-8197, April, pp. 57-91.
5. Medhurst, R.G. (1965) Rainfall attenuation of centimeter waves: comparison of theory and measurement, IEEE Transactions on Antennas and Propagation, AP-13, pp. 550-564.
6. Oguchi, T. (1964) Attenuation of electromagnetic wave due to rain with distorted raindrops (part II), Journal Radio Research Laboratories 11:19-44.
7. Setzer, D.E. (1970) Computed transmission through rain at microwave and visible frequencies, Bell System Technical Journal 49:1873-1892.
8. Crane, R.K. (1974) The rain range experiment–propagation through a simulated rain environment, IEEE Transactions on Antennas and Propagation, AP-22, pp. 321-328.
9. Olsen, R.L., Rogers, D.V., and Hodge, D.B. (1978) The aRb relation in the calculation of rain attenuation, IEEE Transactions on Antennas and Propagation, AP-26, pp. 318-329.
10. Altshuler, E.E. and Telford, L.E. (1980) Frequency Dependence of Slant Path Rain Attenuations at 15 and 35 GHz, paper submitted to Radio Science.
11. Joss, J., Thams, J.C., and Waldvogel, A. (1968) The variation of raindrop size distributions at Locarno, Proceedings of the International Conference on Cloud Physics, Toronto, Canada, pp. 369-373.

12. Llewellyn-Jones, D.T. (1973) Attenuation by rainfall in the submillimetre wave region, Modern Topics in Microwave Propagation and Air-Sea Interaction, A. Zancala, Editor, pp. 285-291.

13. Norbury, J.R. and White, W.J.K. (1973) Correlation Between Measurements of Rainfall Rate and Microwave Attenuation at 36 GHz, Proceedings of IEE Conference on Propagation of Radio Waves at Frequencies Above 10 GHz, No. 98, London, pp. 45-51.

14. Persinger, R.R. and Stutzman, W.L. (1978) Millimeter Wave Propagation Modeling of Inhomogeneous Rain Media For Satellite Communication Systems, Virginia Polytechnic Institute and State University, NASA-CR-156817, June.

15. Hodge, D.B. (1977) Frequency scaling of rain attenuation, IEEE Transcations on Antennas and Propagation, AP-25, pp. 446-447.

16. Crane, R.K. (1967) Coherent pulse transmission through rain, IEEE Transactions on Antennas and Propagation, AP-15, pp. 252-256.

17. Oguchi, T. (1973) Attenuation and phase rotation of radio waves due to rain: calculations at 19.3 and 34.8 GHz, Radio Science 8:31-38.

18. Chu, T.S. (1974) Rain induced cross-polarization at centimeter and millimeter wavelengths, Bell System Technical Journal 53:1557-1580.

19. Slabinski, V.J. (1975) Expression for the time-varying topocentric direction of a geostationary satellite, COMSAT Technical Review 5:1-14.

20. Arnold, H.W., Cox, D.C., Hoffman, H.H., and Leck, R.P. (1979) Rain attenuation statistics from a 19 and 28 GHz COMSTAR beacon propagation experiment: one year cumulative distributions and relationships between two frequencies, IEEE Transactions On Communications, COM-27, pp. 1725-1738.

21. Harris, J.M. and Hyde, G. (1977) Preliminary results of COMSTAR 19/29-GHz beacon measurements at Clarksburg, Maryland, COMSAT Technical Review 7:599-623.

22. Nackoney, O.G. (1979) CTS 11.7 GHz Propagation Measurements, Third Year's Data and Final Report, GTE Laboratories Technical Report TR79-471.3, October.

23. Bergmann, H.J. (1978) A mm-Wave Propagation Experiment in Georgia and Illinois Utilizing COMSTAR Beacon Signals, USNC/URSI Meeting, University of Maryland, May.

24. Tseng, F. and Hyde, G. (1978) Frequency scaling of attenuation above 10-GHz, EASCON, pp. 396-403.

25. Bloch, S.C., Davidson, D., and Tang, D.D. (1978) Rain-attenuation experience with the Tampa triad using 19 GHz COMSTAR satellite beacon signals, EASCON, pp. 379-384.

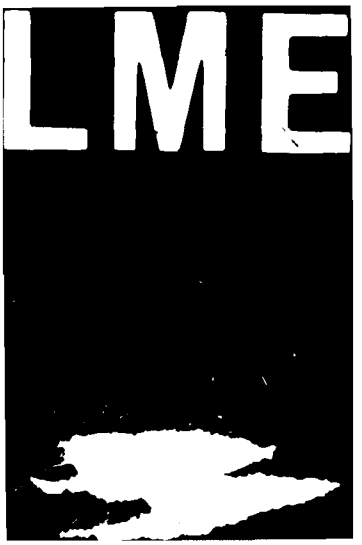
LME